Fast Delocalization Leads To Robust Long-Range Excitonic Transfer in a Large Quantum Chlorosome Model

ARTICLE *in* NANO LETTERS · FEBRUARY 2015

Impact Factor: 13.59 · DOI: 10.1021/nl504399d · Source: PubMed

NANO LETTERS

Letter

pubs.acs.org/NanoLett

Fast Delocalization Leads To Robust Long-Range Excitonic Transfer in a Large Quantum Chlorosome Model

Nicolas P. D. Sawaya,*[,†] Joonsuk Huh,*[,†] Takatoshi Fujita,[†] Semion K. Saikin,[†,‡] and Alán Aspuru-Guzik*[,†]

[†]Department of Chemistry and Chemical Biology, Harvard University, 12 Oxford Street, Cambridge, Massachusetts 02138, United States

[‡]Institute of Physics, Kazan Federal University, 18 Kremlevskaya Street, Kazan 420008, Russian Federation

Supporting Information

ABSTRACT: Chlorosomes are efficient light-harvesting antennas containing up to hundreds of thousands of bacteriochlorophyll molecules. With massively parallel computer hardware, we use a nonperturbative stochastic Schrödinger equation, while including an atomistically derived spectral density, to study excitonic energy transfer in a realistically sized chlorosome model. We find that fast short-range delocalization leads to robust long-range transfer due to the antennae's concentric-roll structure. Additionally, we discover anomalous behavior arising from different initial conditions, and outline general considerations for simulating excitonic systems on the nanometer to micrometer scale.

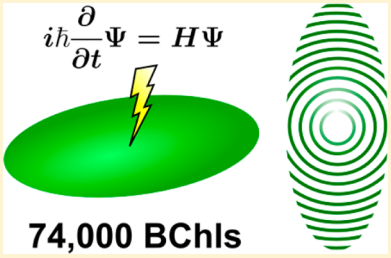

KEYWORDS: *Chlorosome, photosynthesis, green sulfur bacteria, exciton, spectral density, graphics processing unit*

Certain species of green sulfur bacteria can live in water depths of at least 100 m, at which very little light penetrates.[1] These bacteria are thought to be able to survive because of their efficient light-harvesting systems, which contain efficient antennae complexes called chlorosomes. Chlorosomes are large aggregates consisting of tens to hundreds of thousands of bacteriochlorophyll (BChl) molecules. Early experiments demonstrated that these nanoscale self-assembled aggregates are of ellipsoid-shape with semi-principle axis lengths of up to hundreds of nanometers.[2−4] After a photon is absorbed by the chlorosome, the resulting exciton will continue its multistep migration to the reaction center, first moving through the so-called baseplate, a two-dimensional aggregate of protein-bound chromophores. Recent reviews of the chlorosome's structure and function are available.[5,6]

In this theoretical study, we employ a stochastic Schrödinger equation to examine the quantum dynamical excitonic behavior of a realistically sized chlorosome model, while including atomistic bath effects (interactions between nuclear vibrations and excitons) for each molecule. This natural light harvester's impressive size and efficiency make it a relevant object of study, and the inherent limits of spectroscopic methods necessitate the use of computational models to elucidate the physical details of exciton transport. Simulating this very large chlorosome model helps us understand processes occurring on time scales between picoseconds and nanoseconds, provides validation for the proposed structural model, and may point toward design guidelines for artificial light harvesters and other nanoscale electronic devices.[7,8] Another goal of this Letter is to outline important considerations for simulating excitonic systems with length scales between 100 and 1000 nm.

Cryo-EM and NMR experiments have shown that BChl molecules in the chlorosome are packed into lamellar and tubular structures, though the details of both the intralayer molecular packing and the arrangement of the layers themselves have been debated.[9−13] The model used in this paper is a hybrid of concentric rolls and lamellar layers, based on parameters elucidated from a *Chlorobium tepidum* mutant chlorosome (the *bchQ bchR bchU* triple mutant) composed primarily of [8-ethyl,12-methyl]BChl *d*.[10,12−14] Additionally, chlorosomal exciton energy transfer (EET) has been studied experimentally in samples of *Cba. tepidum* using various time-resolved spectroscopy techniques. The picosecond scale time constants are most likely to be relevant to equilibration over an entire roll. Time constants of 10,[15] 12−14,[16] 46−52,[16] and 11 ps[17] were tentatively assigned by the authors to intra-chlorosomal EET. Time constants of 280[15] and 30−40 ps[17] were thought to correspond to EET from the chlorosome to the baseplate.

Several researchers have published theoretical models of exciton dynamics in the chlorosome.[11,15,18−33] Recently, Fujita et al. implemented a chlorosome model of 600 BChl molecules, using a stochastic Schrödinger equation to propagate the system's excitonic wave function.[27,28] They showed that system-bath memory enhances exciton transport, by comparing their method to the Markovian method of Haken, Reineker, and Strobl.[34,35] Valleau et al. simulated the optical behavior of a large model (nearly identical to the structural model of this

Received: November 16, 2014
Revised: February 3, 2015
Published: February 19, 2015

DOI: 10.1021/nl504399d
Nano Lett. 2015, 15, 1722−1729

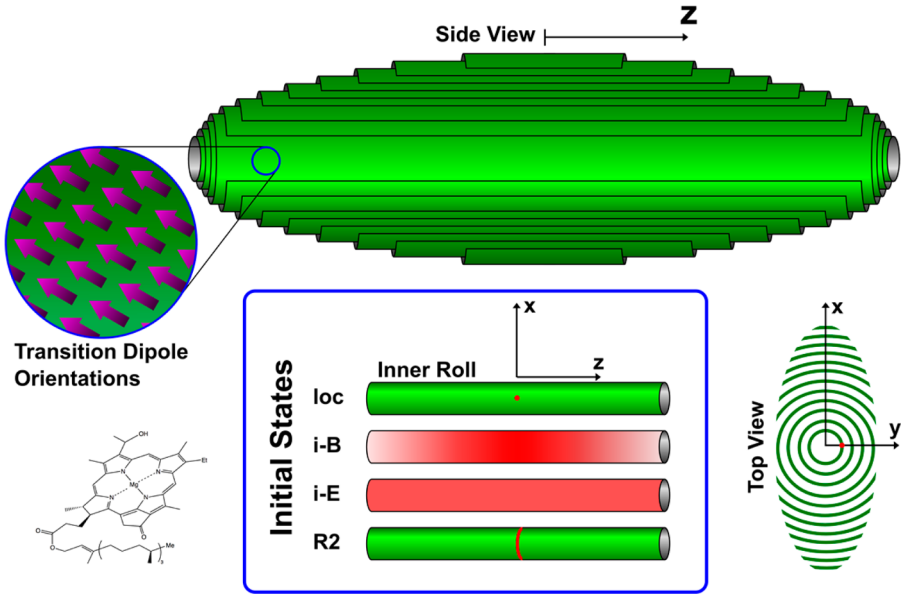

Figure 1. Schematic illustration of the chlorosome model employed in this study. There are four complete rolls, with eight lamellar layers on each side. The transition dipoles are aligned as in ref 36 with a 21 Å spacing between concentric layers. The radius of the innermost roll is 30 Å. Approximate dimensions are 500 × 200 × 1400 Å. All initial states are confined to the inner roll with approximate relative exciton populations shown in red. The *loc* state is localized on a single BChl on the *y*-axis, *i-B* is the eigenstate of the roll's brightest state, *i-E* is evenly distributed among the roll's sites, and *R2* is evenly distributed around the two centermost rings (60 sites). *R2*, *i-E*, and *i-B* are radially symmetric. The chemical structure shown is [8-ethyl,12-methyl]Bchl *d*.

paper) using classical electromagnetic relations,[32] analyzing the significant local field enhancement produced by the chlorosome. Absorption and CD spectra were found to agree with experiment, which provides validation for the model used in this paper. However, their classical model uses single-molecule linear response functions as phenomenological parameters. Thus, using the method for exciton transport modeling would assume a memory-less dissipation process.

Our model, composed entirely of BChl molecules, uses molecular packing parameters from the work of Ganapathy et al. and the layer arrangement of Tang et al.[12,36] It is in the range of a physical chlorosome, which have lengths of 100−200 nm and widths of 10−60 nm.[2−4] These parameters yield a structure of four concentric rolls with eight lamellar layers on each side, as shown in Figure 1. In this work, we will refer to both the rolls and the lamella as sequentially numbered "layers," with the innermost roll labeled 1. The constructed model is of a realistic size, containing approximately 74 000 BChl molecules. This is in agreement with the 50 000 to 250 000 molecules typical of chlorosomes.[37−39] We compare the quantum dynamical behavior that results from four different excitonic initial states (Figure 1), all of which are located on the inner roll.

The chlorosome has a broad absorption spectrum, with appreciable extinction coefficients for frequencies spanning the visible and near IR regions. As a result, it has been shown that green sulfur bacteria can grow under artificial light of narrow spectral width[40] for a range of peak frequencies. In this study, we chose to focus on the excitations resulting from near IR light. Light in this low-energy range primarily excites the Q_y state. Simulating this excited state captures the long-time behavior of excitonic energy transfer, because higher energy initial excitations undergo internal conversion to the Q_y state on a time scale of <300 fs and continue to migrate through the Q-band on the scale of several picoseconds.[6]

Dynamical behavior is qualitatively similar between a concentric roll structure and a hypothetical large rectangular layered structure, because the radius of curvature of most rolls is much larger than the spacing between molecules. In other words, the rolls "look" like flat layers locally. However, one important difference is that the eigenstates of the inner rolls (smaller radius of curvature) are slightly higher in energy, which results in preferential transport to the outer rolls.[11,16]

Though the initial excitonic states of the simulations carried out in this study are coherent superpositions of localized excitons, we emphasize that incoherent light from the sun does not produce coherent initial states. Hence a photosynthetic system does not necessarily behave the same in nature as it does when it is probed with coherent laser light in the laboratory. This difference has been extensively discussed.[41−43] However, laser spectroscopy has been useful in elucidating the behavior of systems like the chlorosome, and thus coherent initial states are very relevant to the interpretation of ultrafast experiments. Additionally, most results from this study either are not dependent on the initial excitation or are dependent only on the spatial position of the initial excitation. Hence these results are applicable to natural light-harvesting conditions in which initial states are incoherent superpositions of the system's eigenstates.

Both the strength of exciton-bath interactions and the excitonic coupling strengths between chromophores have pronounced effects on excitonic behavior. The commonly used Redfield[44−46] theory is valid in the limit of weak system-bath coupling, but sometimes produces unphysical negative population values. Redfield theory has been applied to systems of dimers to several hundreds of molecules.[30,47−50] In contrast, the stochastic Schrödinger equation (SSE) we use is non-perturbative and is thus valid for a wider range of system-bath interaction strengths.[51,52] Note also that the Redfield theory uses a master equation, which is computationally prohibitive for

DOI: 10.1021/nl504399d
Nano Lett. 2015, 15, 1722−1729

large systems because the entire density matrix is propagated. Instead, our SSE propagates the system's state $|\psi\rangle$, which is modeled as a manageable one-dimensional vector.

We also note that the surface hopping method[53−55] would be significantly more computationally expensive for this study, especially if we were to apply an arbitrarily structured spectral density that represents many vibrational modes for all 74 000 sites. Recalculating the nonadiabatic coupling vectors for every time step would be very time-consuming, as it would require the diagonalization of our large and continuously changing effective Hamiltonian.

In our simulations, each monomer is treated as a two-level electronic system, where the excited state is the Q_y state. The effective Hamiltonian of the system, after tracing over the bath degrees of freedom in the interaction representation of the phonon modes,[56] can be written as

$$H(t) = \sum_{n=1}^{N} \{\langle \varepsilon_n \rangle + \Delta\varepsilon_n(t)\}|n\rangle\langle n| + \sum_{n\neq m}^{N} V_{mn}|m\rangle\langle n| \tag{1}$$

where N is the number of sites (BChl molecules), n and m are site indices, $\langle \varepsilon_n \rangle$ is the average site energy, $\Delta\varepsilon_n$ is the fluctuation in the site energy, and V_{mn} is the excitonic coupling between sites m and n. Note that our model does not include excited-state decay, because the excited state lifetime of BChl inside a photosynthetic complex is on the order of nanoseconds.[57] Nor do we include an energy trap for the exciton to funnel to the next part of the photosynthetic chain, because (a) we have studied this process in a recent paper,[30] (b) interlayer transfer occurs on a slightly shorter length scale than transfer to the baseplate, and (c) we are interested in the inherent properties of the isolated concentric roll structure. Off-diagonal terms in the Hamiltonian were calculated using the extended-dipole method[58] with a dipole extent[59] of 8.8 Å and a squared dipole strength of 30 D^2, estimated from experiment by Prokhorenko et al.[15]

For small timesteps, the solution to the time-dependent Schrödinger equation is

$$|\psi(t + dt)\rangle = \exp\left[-\frac{iH(t)dt}{\hbar}\right]|\psi(t)\rangle \tag{2}$$

As the effective system Hamiltonian is very large and is modified at each time step to include bath effects, it is computationally prohibitive to diagonalize the matrix at every time step. For accuracy and stability, we used an exponential integrator instead of an Euler or classical Runge−Kutta method. The exponentiation was implemented using the Lanczos decomposition,[60,61] a so-called Krylov subspace method, making it possible to use the Schrödinger equation to propagate even very large quantum systems. We then use the Padè approximant (as implemented in the CULA package[62]). Our GPU-based implementation was written using CUDA, following the algorithm and error analysis used in the software package EXPOKIT.[63]

The spectral density, which describes exciton-bath interactions, is often approximated as having, for example, an Ohmic form.[56,64] However, the true spectral density can be significantly more structured, being composed of several well-separated peaks. It can also change appreciably depending on whether the molecule is in solution or in aggregate, and on which protein or molecular environment surrounds the molecule.[65] We use a method to incorporate the detailed "structured" spectral density (SSD). Our spectral density was previously determined from atomistic QM/MM (quantum mechanics/molecular mechanics) calculations, which provides a more realistic description of system-bath interactions than using an approximate analytical form.[27,28,66] This spectral density was calculated for a BChl molecule of a smaller multiroll chlorosome model, where the local environment is identical to that of our large model. Fluctuations in the Hamiltonian are calculated as[51]

$$\Delta\varepsilon_n(t) = \sum_{i=1}^{N_{ph}} [f_n(\omega_i)\Delta\omega]^{1/2}\cos(\omega_i t + \phi_i) \tag{3}$$

where N_{ph} is the number of oscillators used to model bath interactions, ϕ_n are random phases drawn uniformly and independently from the interval $[0, 2\pi)$, ω_n are the frequencies of oscillation, and $\Delta\omega$ is an arbitrary discretization parameter. The function $f_n(\omega_i)$ depends on both temperature and the arbitrarily shaped spectral density. We use the harmonic prefactor in calculating the spectral density.[67] Static disorder, which accounts for structural defects and variations between chlorosomes, was modeled as described previously.[27,28]

We compare this approach to our previously implemented method, in which the site energy fluctuations are propagated using the Langevin equation

$$\frac{\partial}{\partial t}\Delta\varepsilon_n = -\frac{\Delta\varepsilon_n}{\tau_n} + F_n(t) \tag{4}$$

where the relaxation time τ_n and the stochastic force $F_n(t)$ are determined as previously described.[27,28] This method is equivalent to the Kubo−Anderson model (KA).[68,69] τ and $\langle\Delta\varepsilon^2\rangle$ were averaged from the syn and anti BChl parameters calculated previously.[27,28]

To save memory and computation time in modeling a system with thousands of sites, it is necessary to enforce sparsity by neglecting coupling values for which $V_{mn} \leq E_{cut}$. Note that long-range interactions between transition dipoles scale as r^{-3}. This energy cutoff E_{cut} must be chosen carefully for large three-dimensional systems. Though the dynamical behavior converges quickly in 1D and 2D, we saw significantly slower convergence in 3D. We used two criteria to guarantee that the system's behavior was converged. First, we ensured that for each site n, coherent effects were not neglected. We required that $\sum_{m\,(\mathrm{negl})} V_{mn}^2 \leq (k_B T)^2$, where the sum is over the neglected site couplings m(negl), k_B is the Boltzmann constant, and T is the temperature. Second, we confirmed that the relative probability of incoherent hopping from site n to a neglected site was less than 2%, such that $\sum_{m\,(\mathrm{negl})} V_{mn}^2 / \sum_m V_{mn}^2 < 0.02$. A surprisingly low cutoff value of 1 cm^{-1} was required to meet the two criteria. We verified that the model's dynamical behavior was converged at this cutoff. The final excitonic Hamiltonian matrix contained approximately 28 million nonzero elements for a matrix sparsity of ∼0.5%. Along with efficient Krylov subspace propagation methods, this cutoff criteria is an important consideration for the study other large excitonic and electronic systems including quantum dot arrays,[70] organic photovoltaics,[71,72] and dye-functionalized DNA structures.[8,73,74]

Simulations were run on NVIDIA K20 graphics processing units (GPUs). We compared the computational performance to a modified MPI version of EXPOKIT.[63] Our GPU code achieved a 6−7× speedup over a 32-core node of AMD Opteron 6376 processors.

DOI: 10.1021/nl504399d
Nano Lett. 2015, 15, 1722−1729

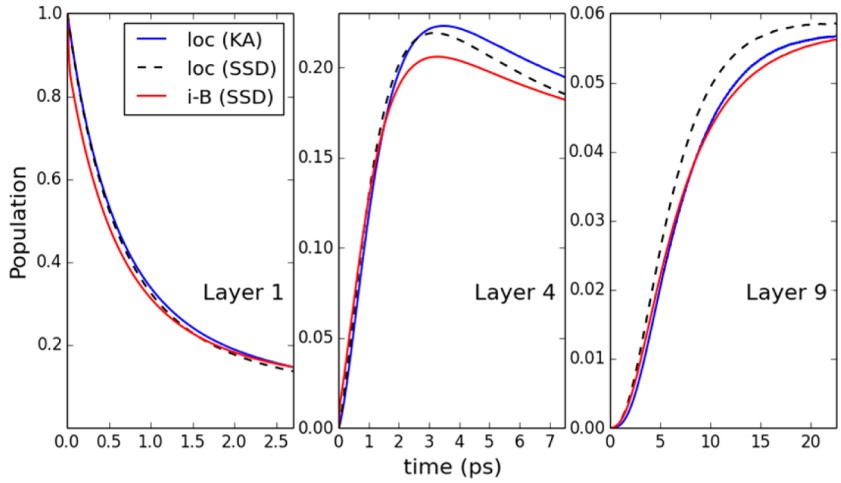

Figure 2. Time-dependent exciton populations in select layers. KA and SSD refer to the Kubo−Anderson model and the structured spectral density model, respectively. The exciton migrates more quickly in the SSD model than in the KA model. Excitonic energy transfer from the state *i-B* is faster for the first several hundred femtoseconds, but transfer beginning from *loc* reaches the outer layers more quickly.

Sample exciton populations are shown in Figure 2. Though exciton migration is not a strictly diffusive process, we calculate phenomenological "diffusion parameters" from the derivatives of the exciton's mean square displacement. Diffusion parameters are shown in Figure 4, calculated at 20 fs to compare early diffusive behavior. Axial (D_Z) diffusion parameters are comparable to values found for artificial aggregates of cyanine dyes,[75] while the interlayer radial (D_R) diffusion parameters of initially delocalized states are several times smaller. Because of closer molecular spacing, the exciton travels 2−4 times faster in the axial than the radial direction. This is desirable as the chlorosome is longer in the axial direction. Slower incoherent transport occurs along the radial direction, because the larger distance between layers results in smaller excitonic coupling values. This provides insight into the dimensions of the chlorosome: if a similar ellipsoid's rolls were oriented along one of the minor axes, EET along its longest direction would occur more slowly.

To compare exciton transport speed between models, we calculated the time for the population of the 11th layer to reach 90% of its final value (Figure 4). Exciton dynamics in the model were robust to temperature changes, with simulations at 77 (not shown) and 300 K producing both equilibration times and diffusion parameters that agree within 4%. The equilibration times reported here from 11−21 ps are consistent with experimental time constants ranging from 12−280 ps,[15−17] because these computations provide a lower bound for the time it takes to reach the baseplate from the center roll. Our equilibration time scales are shorter than some of the experimental values. This is consistent with the exciton sitting on the outer regions of the chlorosome for several picoseconds, before funneling to the lower-energy chromophores of the baseplate.[30]

Beginning from the *loc* state, SSD simulations resulted in faster transport when compared to the KA model. For example, D_Z and D_R from the SSD model are larger than those from the KA model by 15 and 14%, respectively. This is despite the comparable values between calculated standard deviations of the site fluctuations, 523 cm^{-1} for the SSD model and 539 cm^{-1} for the KA model. Note that Fujita's KA model, eq 4, is equivalent to using eq 3 with a Drude-Lorenz spectral density[76] peaked at $\omega \approx 800$ cm^{-1}, while our structured spectral density is concentrated between 1500 and 1900 cm^{-1}.[27,28] It is well-known that for a given fluctuation magnitude, lower frequency fluctuations inhibit exciton dynamics more.[56,64] This is because higher-frequency fluctuations result in more frequent site energy overlap, during which the resonance condition is met. Phrased less formally, the site energies are close in value for a larger fraction of time. These differences in transport times suggest that for the simulation of some large systems, it is important to include all information contained in the spectral density.

The 300 K SSD model was used to run simulations starting from our four initial states (Figure 3). D_Z was calculated to be 123 and 162 nm^2/ps for initial states *loc* and *R*2, respectively, for an increase of over 30%. Note that these two states are centrally located along the *z*-axis. This increase in transfer rate is well-known to occur in coherently delocalized states, whether the transfer itself is coherent or incoherent.[41,77,78] However, interlayer dynamics are nearly identical for these two initial states, partly because the time scale for intraroll transfer is smaller than the time scale for inter-roll transfer. Hence initially localized excitations appear to be transferred nearly as efficiently as delocalized ones, as a result of this difference in time scales.

This result suggests that intraroll delocalization may lead to robust incoherent inter-roll energy transfer. Throughout this letter we use the term "robust" to mean that a process (long-range inter-roll exciton transfer) is relatively unaffected by changes in a parameter or property, which in this case means by changes in the initial state. Note also that although equilibration times differ for the four initial states, similar qualitative behavior is observed for all states after the fast transfer that occurs during the first tens of femtoseconds. This robustness to the initial state suggests that despite structural defects that may produce localized excitons, the concentric roll structure is still capable of efficiently funneling the exciton to the lower-energy collective states of the outer layers.[11]

The two initial states that are delocalized in the axial (z) direction, *i-B* and *i-E*, enhance radial transport for the first ∼40 fs (Figure 3) when compared to *R*2. This may be because the delocalized excitons are more strongly coupled to the bright eigenstate of the second roll, which is similar in shape to *i-E*. However, this trend soon reverses. Excitons from *i-B* and *i-E*

DOI: 10.1021/nl504399d
Nano Lett. 2015, 15, 1722−1729

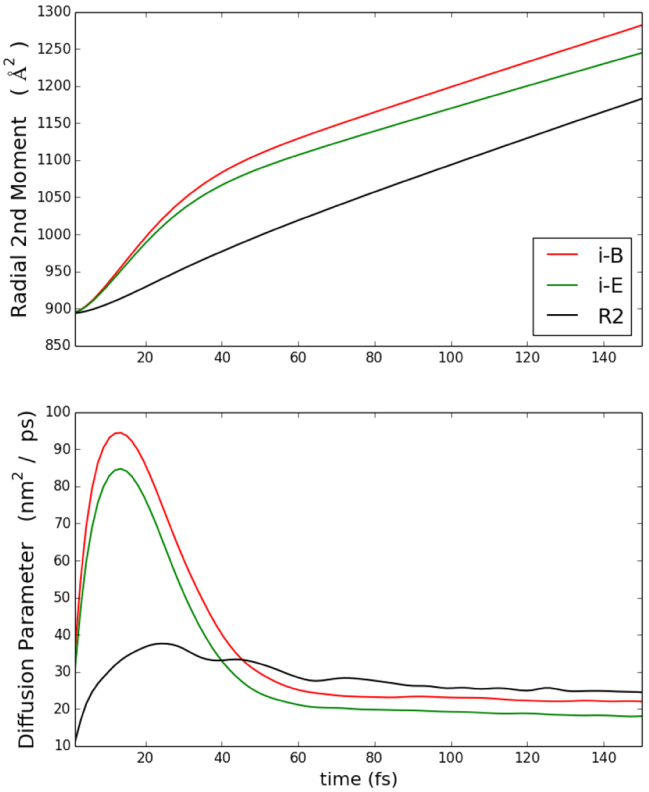

Figure 3. Top: Radial second moments from three delocalized initial states. The state *loc* is omitted because its initial radial diffusion results from intraroll transfer. Bottom: Time-dependent diffusion parameters for each state. The diffusion parameter for *R*2 remains larger than the others, so that the *R*2 simulation's radial second moment eventually overtakes the *i-B* and *i-E* simulations.

ultimately reach the radial extremes more slowly than *R*2 and *loc*. The chlorosome model's ellipsoid shape is responsible for this time difference, because the portion of the exciton population that is concentrated at the axial extremes is coupled to fewer sites. For example, an exciton located near the edge of the chlorosome (at $z \approx 700$ Å) is coupled to fewer sites than one located in the center (at $z \approx 0$ Å), and thus migrates more slowly. This effect becomes more pronounced as the exciton moves radially, because the layer heights (z lengths) decrease at a faster rate. On the other hand, the simulations from *loc* and *R*2 equilibrate faster because they are concentrated at the chlorosome's vertical center. Considering that *i-E* is more centrally concentrated than *i-B*, we observe the expected trend in equilibration rates, *i-E* < *i-B* < *R*2 ∼ *loc*. This differs from the early transfer speed trend of *R*2 < *i-E* < *i-B* seen in Figure 4. The ellipsoid shape is likely the result of an array of biological factors, but these simulations hint at design principles for artificial light-harvesting aggregates. The exciton would be less hindered, for example, if all concentric rolls were of equal length, forming a single large cylinder instead of an ellipsoid.

We studied the quantum dynamical behavior of a realistically sized chlorosome model containing approximately 74 000 BChl molecules. To our knowledge, this is the largest excitonic system that has been studied by directly implementing the time-dependent Schrödinger equation. The initial excitation's character was shown to affect both short time and long time dynamics, often in contradictory ways. However, the long-range transfer was robust to the initial excited state because of fast intraroll equilibration, demonstrating the advantage of the chlorosome's concentric multilayer design. Using a structured spectral density resulted in appreciable dynamical differences when compared to a more simplistic bath model based on the Langevin equation. The approach of using parallel hardware and Krylov subspace exponentiation methods can be used to account for quantum effects and arbitrary bath effects in other large excitonic systems on the order of hundreds of nanometers, including bulk heterojunction solar cells and organic light-emitting diodes.

■ ASSOCIATED CONTENT

Ⓢ Supporting Information

Simulation parameters; details concerning bath fluctuation calculations; additional plots of second moments and populations; and analysis of exciton delocalization. This material is available free of charge via the Internet at http://pubs.acs.org.

■ AUTHOR INFORMATION

Corresponding Authors

*E-mail: (N.P.D.S.) nicolassawaya@fas.harvard.edu.
*E-mail: (J.H.) huh@fas.harvard.edu.
*E-mail: (A.A.-G.) aspuru@chemistry.harvard.edu.

Notes

The authors declare no competing financial interest.

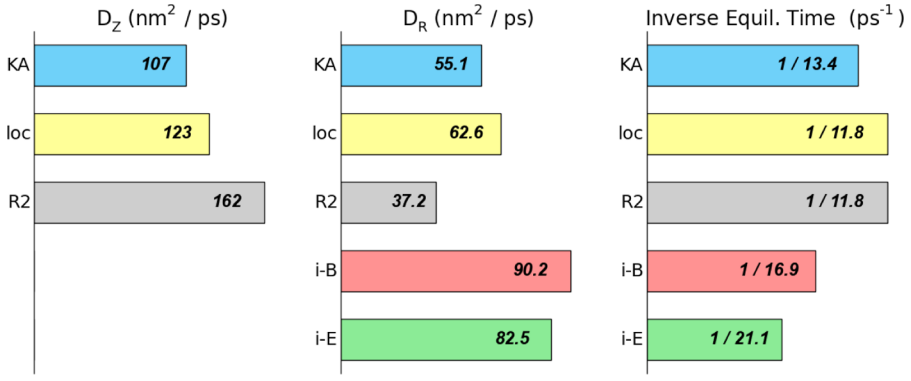

Figure 4. Equilibration time is arbitrarily defined as the time at which the 11th layer reaches 90% of the equilibration population. Diffusion parameter D_R and D_Z (radial and axial, respectively) were calculated at $t = 20$ fs to capture early diffusive behavior. States *i-B* and *i-E* are already delocalized in the *z*-direction. The KA simulation begins with initial state *loc*. All other simulations use the SSD model at 300 K. Note the reversal in some trends between short time (first and second column) and long time (third column) behavior.

DOI: 10.1021/nl504399d
Nano Lett. 2015, 15, 1722−1729

■ ACKNOWLEDGMENTS

We are grateful for fruitful conversations with Stephanie Valleau about the spectral density. N.S., J.H., T.F., and A.A.-G. acknowledge support from the Center for Excitonics, an Energy Frontier Research Center funded by the U.S. Department of Energy under award DE-SC0001088. The majority of our computations were run on Harvard University's Odyssey cluster, supported by the Research Computing Group of the FAS Division of Science. N.S. thanks the Smith Family Graduate Science and Engineering Fellowship for financial support. J.H., S.S., and A.A.-G. also acknowledge Defense Threat Reduction Agency Grant HDTRA1-10-1-0046 and the Air Force Office of Scientific Research Grant FA9550-12-1-0046. S.S. also acknowledges the support from the subsidy allocated to Kazan Federal University for performing the state assignment in the area of scientific activities. Further, A.A.-G. is grateful for support from Defense Advanced Research Projects Agency Grant N66001-10-1-4063, as well as for generous support from the Corning Foundation. Some of the hardware used for this project was provided by NVIDIA's CUDA Center of Excellence (CCOE) Program.

■ REFERENCES

(1) Manske, A. K.; Glaeser, J.; Kuypers, M. M. M.; Overmann, J. Physiology and Phylogeny of Green Sulfur Bacteria Forming a Monospecific Phototrophic Assemblage at a Depth of 100 Meters in the Black Sea. *Appl. Environ. Microbiol.* **2005**, *71* (12), 8049−8060.

(2) Cohen-Bazire, G.; Pfennig, N.; Kunisawa, R. The Fine Structure of Green Bacteria. *J. Cell Biol.* **1964**, *22* (1), 207−225.

(3) Staehelin, A. L.; Golecki, J. R.; Drews, G. Supramolecular organization of chlorosomes (chlorobium vesicles) and of their membrane attachment sites in Chlorobium Limicola. *Biochim. Biophys. Acata, Bioenerg.* **1980**, *589* (1), 30−45.

(4) Staehelin, L. A.; Golecki, J.; Fuller, R. C.; Drews, G. Visualization of the supramolecular architecture of chlorosomes (chlorobium type vesicles) in freeze-fractured cells of Chloroflexus aurantiacus. *Arch. Microbiol.* **1978**, *119* (3), 269−277.

(5) Oostergetel, G.; van Amerongen, H.; Boekema, E. The chlorosome: a prototype for efficient light harvesting in photosynthesis. *Photosynth. Res.* **2010**, *104* (2−3), 245−255.

(6) Orf, G.; Blankenship, R. Chlorosome antenna complexes from green photosynthetic bacteria. *Photosynth. Res.* **2013**, *116* (2−3), 315−331.

(7) Eisele, D. M.; Cone, C. W.; Bloemsma, E. A.; Vlaming, S. M.; van der Kwaak, C. G. F.; Silbey, R. J.; Bawendi, M. G.; Knoester, J.; Rabe, J. P.; Vanden Bout, D. A. Utilizing redox-chemistry to elucidate the nature of exciton transitions in supramolecular dye nanotubes. *Nat. Chem.* **2012**, *4* (8), 655−662.

(8) Schwartz, E.; Le Gac, S.; Cornelissen, J. J. L. M.; Nolte, R. J. M.; Rowan, A. E. Macromolecular multi-chromophoric scaffolding. *Chem. Soc. Rev.* **2010**, *39* (5), 1576−1599.

(9) Pšenčík, J.; Ikonen, T. P.; Laurinmäki, P.; Merckel, M. C.; Butcher, S. J.; Serimaa, R. E.; Tuma, R. Lamellar Organization of Pigments in Chlorosomes, the Light Harvesting Complexes of Green Photosynthetic Bacteria. *Biophys. J.* **2004**, *87* (2), 1165−1172.

(10) Oostergetel, G. T.; Reus, M.; Gomez Maqueo Chew, A.; Bryant, D. A.; Boekema, E. J.; Holzwarth, A. R. Long-range organization of bacteriochlorophyll in chlorosomes of Chlorobium tepidum investigated by cryo-electron microscopy. *FEBS Lett.* **2007**, *581* (28), 5435−5439.

(11) Linnanto, J.; Korppi-Tommola, J. I. Investigation on chlorosomal antenna geometries: tube, lamella and spiral-type self-aggregates. *Photosynth. Res.* **2008**, *96* (3), 227−245.

(12) Ganapathy, S.; Oostergetel, G. T.; Wawrzyniak, P. K.; Reus, M.; Gomez Maqueo Chew, A.; Buda, F.; Boekema, E. J.; Bryant, D. A.; Holzwarth, A. R.; de Groot, H. J. M. Alternating syn-anti bacteriochlorophylls form concentric helical nanotubes in chlorosomes. *Proc. Natl. Acad. Sci. U.S.A.* **2009**, *106* (21), 8525−8530.

(13) Ganapathy, S.; Oostergetel, G. T.; Reus, M.; Tsukatani, Y.; Gomez Maqueo Chew, A.; Buda, F.; Bryant, D. A.; Holzwarth, A. R.; de Groot, H. J. M. Structural Variability in Wild-Type and *bchQ bchR* Mutant Chlorosomes of the Green Sulfur Bacterium *Chlorobaculum tepidum*. *Biochemistry* **2012**, *51* (22), 4488−4498.

(14) Chew, A. G. M.; Bryant, D. A. Chlorophyll Biosynthesis in Bacteria: The Origins of Structural and Functional Diversity. *Annu. Rev. Microbiol.* **2007**, *61* (1), 113−129.

(15) Prokhorenko, V. I.; Steensgaard, D. B.; Holzwarth, A. R. Exciton Dynamics in the Chlorosomal Antennae of the Green Bacteria Chloroflexus aurantiacus and Chlorobium tepidum. *Biophys. J.* **2000**, *79* (4), 2105−2120.

(16) Martiskainen, J.; Linnanto, J.; Aumanen, V.; Myllyperkiö, P.; Korppi-Tommola, J. Excitation Energy Transfer in Isolated Chlorosomes from Chlorobaculum tepidum and Prosthecochloris aestuarii. *Photochem. Photobiol.* **2012**, *88* (3), 675−683.

(17) Pšenčík, J.; Polívka, T.; Němec, P.; Dian, J.; Kudrna, J.; Malý, P.; Hála, J. Fast Energy Transfer and Exciton Dynamics in Chlorosomes of the Green Sulfur Bacterium *Chlorobium tepidum*. *J. Phys. Chem. A* **1998**, *102* (23), 4392−4398.

(18) Alden, R. G.; Lin, S. H.; Blankenship, R. E. Theory of spectroscopy and energy transfer of oligomeric pigments in chlorosome antennas of green photosynthetic bacteria. *J. Lumin.* **1992**, *51* (1−3), 51−66.

(19) Novoderezhkin, V. I.; Fetisova, Z. G. Structure of bacteriochlorophyll aggregates in chlorosomes of green bacteria: A spectral hole burning study. *IUBMB Life* **1996**, *40* (2), 243−252.

(20) Mizoguchi, T.; Hara, K.; Nagae, H.; Koyama, Y. Structural Transformation Among the Aggregate Forms of Bacteriochlorophyll c as Determined by Electronic-Absorption and NMR Spectroscopies: Dependence on the Stereoisomeric Configuration and on the Bulkiness of the 8-C Side Chain. *Photochem. Photobiol.* **2000**, *71* (5), 596−609.

(21) Novoderezhkin, V.; Taisova, A.; Fetisova, Z. G. Unit building block of the oligomeric chlorosomal antenna of the green photosynthetic bacterium Chloroflexus aurantiacus: modeling of nonlinear optical spectra. *Chem. Phys. Lett.* **2001**, *335* (3−4), 234−240.

(22) Didraga, C.; Knoester, J. Absorption and dichroism spectra of cylindrical J aggregates and chlorosomes of green bacteria. *J. Lumin.* **2003**, *102−103* (0), 60−66.

(23) Prokhorenko, V. I.; Steensgaard, D. B.; Holzwarth, A. R. Exciton Theory for Supramolecular Chlorosomal Aggregates: 1. Aggregate Size Dependence of the Linear Spectra. *Biophys. J.* **2003**, *85* (5), 3173−3186.

(24) Pšenčík, J.; Ma, Y.-Z.; Arellano, J. B.; Hála, J.; Gillbro, T. Excitation Energy Transfer Dynamics and Excited-State Structure in Chlorosomes of Chlorobium phaeobacteroides. *Biophys. J.* **2003**, *84* (2), 1161−1179.

(25) Linnanto, J. M.; Korppi-Tommola, J. E. I. Modelling excitonic energy transfer in the photosynthetic unit of purple bacteria. *Chem. Phys.* **2009**, *357* (1−3), 171−180.

(26) Pajusalu, M.; Rätsep, M.; Trinkunas, G.; Freiberg, A. Davydov Splitting of Excitons in Cyclic Bacteriochlorophyll a Nanoaggregates of Bacterial Light-Harvesting Complexes between 4.5 and 263 K. *ChemPhysChem* **2011**, *12* (3), 634−644.

(27) Fujita, T.; Brookes, J. C.; Saikin, S. K.; Aspuru-Guzik, A. Memory-Assisted Exciton Diffusion in the Chlorosome Light-Harvesting Antenna of Green Sulfur Bacteria. *J. Phys. Chem. Lett.* **2012**, *3* (17), 2357−2361.

(28) Fujita, T.; Huh, J.; Saikin, S.; Brookes, J.; Aspuru-Guzik, A. Theoretical characterization of excitation energy transfer in chlorosome light-harvesting antennae from green sulfur bacteria. *Photosynth. Res.* **2014**, *120* (3), 273−289.

(29) Linnanto, J. M.; Korppi-Tommola, J. E. I. Exciton Description of Chlorosome to Baseplate Excitation Energy Transfer in Filamentous Anoxygenic Phototrophs and Green Sulfur Bacteria. *J. Phys. Chem. B* **2013**, *117* (38), 11144−11161.

DOI: 10.1021/nl504399d
Nano Lett. 2015, 15, 1722−1729

(30) Huh, J.; Saikin, S. K.; Brookes, J. C.; Valleau, S.; Fujita, T.; Aspuru-Guzik, A. Atomistic Study of Energy Funneling in the Light-Harvesting Complex of Green Sulfur Bacteria. *J. Am. Chem. Soc.* **2014**, *136* (5), 2048−2057.
(31) Nalbach, P. Coherent or hopping like energy transfer in the chlorosome? *AIP Conf. Proc.* **2014**, *1610* (1), 135−140.
(32) Valleau, S.; Saikin, S. K.; Ansari-Oghol-Beig, D.; Rostami, M.; Mossallaei, H.; Aspuru-Guzik, A. Electromagnetic Study of the Chlorosome Antenna Complex of Chlorobium tepidum. *ACS Nano* **2014**, *8* (4), 3884−3894.
(33) Wan, Y.; Stradomska, A.; Fong, S.; Guo, Z.; Schaller, R. D.; Wiederrecht, G. P.; Knoester, J.; Huang, L. Exciton Level Structure and Dynamics in Tubular Porphyrin Aggregates. *J. Phys. Chem. C* **2014**, *118* (43), 24854−24865.
(34) Haken, H.; Reineker, P. The coupled coherent and incoherent motion of excitons and its influence on the line shape of optical absorption. *Z. Phys.* **1972**, *249* (3), 253−268.
(35) Haken, H.; Strobl, G. An exactly solvable model for coherent and incoherent exciton motion. *Z. Phys.* **1973**, *262* (2), 135−148.
(36) Tang, J. K.-H.; Saikin, S. K.; Pingali, S. V.; Enriquez, M. M.; Huh, J.; Frank, H. A.; Urban, V. S.; Aspuru-Guzik, A. Temperature and Carbon Assimilation Regulate the Chlorosome Biogenesis in Green Sulfur Bacteria. *Biophys. J.* **2013**, *105* (6), 1346−1356.
(37) Martinez-Planells, A.; Arellano, J.; Borrego, C.; López-Iglesias, C.; Gich, F.; Garcia-Gil, J. Determination of the topography and biometry of chlorosomes by atomic force microscopy. *Photosynth. Res.* **2002**, *71* (1−2), 83−90.
(38) Montaño, G. A.; Bowen, B. P.; LaBelle, J. T.; Woodbury, N. W.; Pizziconi, V. B.; Blankenship, R. E. Characterization of Chlorobium tepidum Chlorosomes: A Calculation of Bacteriochlorophyll c per Chlorosome and Oligomer Modeling. *Biophys. J.* **2003**, *85* (4), 2560−2565.
(39) Saga, Y.; Shibata, Y.; Itoh, S.; Tamiaki, H. Direct Counting of Submicrometer-Sized Photosynthetic Apparatus Dispersed in Medium at Cryogenic Temperature by Confocal Laser Fluorescence Microscopy: Estimation of the Number of Bacteriochlorophyll *c* in Single Light-Harvesting Antenna Complexes Chlorosomes of Green Photosynthetic Bacteria. *J. Phys. Chem. B* **2007**, *111* (43), 12605−12609.
(40) Saikin, S. K.; Khin, Y.; Huh, J.; Hannout, M.; Wang, Y.; Zare, F.; Aspuru-Guzik, A.; Tang, J. K.-H. Chromatic acclimation and population dynamics of green sulfur bacteria grown with spectrally tailored light. *Sci. Rep.* **2014**, *4*, 5057.
(41) Kassal, I.; Yuen-Zhou, J.; Rahimi-Keshari, S. Does Coherence Enhance Transport in Photosynthesis? *J. Phys. Chem. Lett.* **2013**, *4* (3), 362−367.
(42) Ishizaki, A.; Fleming, G. R. Quantum Coherence in Photosynthetic Light Harvesting. *Annu. Rev. Condens. Matter Phys.* **2012**, *3* (1), 333−361.
(43) Pelzer, K. M.; Can, T.; Gray, S. K.; Morr, D. K.; Engel, G. S. Coherent Transport and Energy Flow Patterns in Photosynthesis under Incoherent Excitation. *J. Phys. Chem. B* **2014**, *118* (10), 2693−2702.
(44) Ishizaki, A.; Fleming, G. R. On the adequacy of the Redfield equation and related approaches to the study of quantum dynamics in electronic energy transfer. *J. Chem. Phys.* **2009**, *130* (23), 234110.
(45) Redfield, A. G. On the Theory of Relaxation Processes. *IBM J. Res. Dev.* **1957**, *1*, 19.
(46) Redfield, A. G. The Theory of Relaxation Processes. *Adv. Magn. Reson.* **1965**, *1*, 1.
(47) Duffy, C. D. P.; Ruban, A. V.; Barford, W. Theoretical Investigation of the Role of Strongly Coupled Chlorophyll Dimers in Photoprotection of LHCII. *J. Phys. Chem. B* **2008**, *112* (39), 12508−12515.
(48) Novoderezhkin, V. I.; Palacios, M. A.; van Amerongen, H.; van Grondelle, R. Energy-Transfer Dynamics in the LHCII Complex of Higher Plants: Modified Redfield Approach. *J. Phys. Chem. B* **2004**, *108* (29), 10363−10375.
(49) Warshel, A. Role of the chlorophyll dimer in bacterial photosynthesis. *Proc. Natl. Acad. Sci. U.S.A.* **1980**, *77* (6), 3105−3109.
(50) Warshel, A. The Origin of the Red Shift of the Absorption Spectra of Aggregated Chlorophylls. *J. Am. Chem. Soc.* **1979**, *101* (3), 744−746.
(51) Zhong, X.; Zhao, Y. Charge carrier dynamics in phonon-induced fluctuation systems from time-dependent wavepacket diffusion approach. *J. Chem. Phys.* **2011**, *135* (13), 134110.
(52) Zhong, X.; Zhao, Y. Non-Markovian stochastic Schrödinger equation at finite temperatures for charge carrier dynamics in organic crystals. *J. Chem. Phys.* **2013**, *138* (1), 014111.
(53) Tully, J. C. Molecular dynamics with electronic transitions. *J. Chem. Phys.* **1990**, *93* (2), 1061−1071.
(54) Dahlbom, M.; Beenken, W.; Sundström, V.; Pullerits, T. Collective excitation dynamics and polaron formation in molecular aggregates. *Chem. Phys. Lett.* **2002**, *364* (5−6), 556−561.
(55) Beenken, W. J. D.; Dahlbom, M.; Kjellberg, P.; Pullerits, T. Potential surfaces and delocalization of excitons in dimers. *J. Chem. Phys.* **2002**, *117* (12), 5810−5820.
(56) May, V.; Kühn, O. *Charge and Energy Transfer Dynamics in Molecular Systems*, 3rd ed.; Wiley-VCH: Berlin, 2011.
(57) Govindjee; Hammond, J. H.; Merkelo, H. Lifetime of the Excited State In Vivo: II. Bacteriochlorophyll in Photosynthetic Bacteria at Room Temperature. *Biophys. J.* **1972**, *12* (7), 809−814.
(58) Czikklely, V.; Forsterling, H. D.; Kuhn, H. Extended dipole model for aggregates of dye molecules. *Chem. Phys. Lett.* **1970**, *6* (3), 207−210.
(59) Madjet, M. E.; Abdurahman, A.; Renger, T. Intermolecular Coulomb Couplings from Ab Initio Electrostatic Potentials: Application to Optical Transitions of Strongly Coupled Pigments in Photosynthetic Antennae and Reaction Centers. *J. Phys. Chem. B* **2006**, *110* (34), 17268−17281.
(60) Lanczos, C. An Iteration Method for the Solution of the Eigenvalue Problem of Linear Differential and Integral Operators. *J. Res. Natl. Bur. Stand. (U. S.)* **1950**, *45* (4), 255.
(61) Park, T. J.; Light, J. C. Unitary quantum time evolution by iterative Lanczos reduction. *J. Chem. Phys.* **1986**, *85* (10), 5870−5876.
(62) Humphrey, J. R.; Price, D. K.; Spagnoli, K. E.; Paolini, A. L.; Kelmelis, E. J. CULA: Hybrid GPU Accelerated Linear Algebra Routines. *Proc. SPIE* **2010**, DOI: 10.1117/12.850538.
(63) Sidje, R. B. EXPOKIT: Software Package for Computing Matrix Exponentials. *ACM Trans. Math. Softw.* **1998**, *24* (1), 130−156.
(64) Leggett, A. J.; Chakravarty, S.; Dorsey, A. T.; Fisher, M. P. A.; Garg, A.; Zwerger, W. Dynamics of the dissipative two-state system. *Rev. Mod. Phys.* **1987**, *59* (1), 1−85.
(65) Olbrich, C.; Strümpfer, J.; Schulten, K.; Kleinekathöfer, U. Theory and Simulation of the Environmental Effects on FMO Electronic Transitions. *J. Phys. Chem. Lett.* **2011**, *2* (14), 1771−1776.
(66) Mercer, I. P.; Gould, I. R.; Klug, D. R. A Quantum Mechanical/Molecular Mechanical Approach to Relaxation Dynamics: Calculation of the Optical Properties of Solvated Bacteriochlorophyll-a. *J. Phys. Chem. B* **1999**, *103* (36), 7720−7727.
(67) Valleau, S.; Eisfeld, A.; Aspuru-Guzik, A. On the alternatives for bath correlators and spectral densities from mixed quantum-classical simulations. *J. Chem. Phys.* **2012**, *137* (22), 224103.
(68) Anderson, P. W. A Mathematical Model for the Narrowing of Spectral Lines by Exchange or Motion. *J. Phys. Soc. Jpn.* **1954**, *9* (3), 316−339.
(69) Kubo, R. Note on the Stochastic Theory of Resonance Absorption. *J. Phys. Soc. Jpn.* **1954**, *9* (6), 935−944.
(70) Matsueda, H.; Leosson, K.; Xu, Z.; Hvam, J. M.; Ducommun, Y.; Hartmann, A.; Kapon, E. Dynamic dipole-dipole interactions between excitons in quantum dots of different sizes. *IEEE Trans. Nanotechnol.* **2004**, *3* (2), 318−327.
(71) Nelson, J. Polymer:fullerene bulk heterojunction solar cells. *Mater. Today* **2011**, *14* (10), 462−470.
(72) Heeger, A. J. 25th Anniversary Article: Bulk Heterojunction Solar Cells: Understanding the Mechanism of Operation. *Adv. Mater. (Weinheim, Ger.)* **2014**, *26* (1), 10−28.

DOI: 10.1021/nl504399d
Nano Lett. 2015, 15, 1722−1729

(73) Asanuma, H.; Fujii, T.; Kato, T.; Kashida, H. Coherent interactions of dyes assembled on DNA. *J. Photochem. Photobiol. C* **2012**, *13* (2), 124−135.
(74) Pan, K.; Boulais, E.; Yang, L.; Bathe, M. Structure-based model for light-harvesting properties of nucleic acid nanostructures. *Nucleic Acids Res.* **2014**, *42* (4), 2159−2170.
(75) Valleau, S.; Saikin, S. K.; Yung, M.-H.; Guzik, A. A. Exciton transport in thin-film cyanine dye J-aggregates. *J. Chem. Phys.* **2012**, *137* (3), 034109.
(76) Ishizaki, A.; Calhoun, T. R.; Schlau-Cohen, G. S.; Fleming, G. R. Quantum coherence and its interplay with protein environments in photosynthetic electronic energy transfer. *Phys. Chem. Chem. Phys.* **2010**, *12* (27), 7319−7337.
(77) Abasto, D. F.; Mohseni, M.; Lloyd, S.; Zanardi, P. Exciton diffusion length in complex quantum systems: the effects of disorder and environmental fluctuations on symmetry-enhanced supertransfer. *Philos. Trans. R. Soc., A* **2012**, *370* (1972), 3750−3770.
(78) Lloyd, S.; Mohseni, M. Symmetry-enhanced supertransfer of delocalized quantum states. *New J. Phys.* **2010**, *12* (7), 075020.

DOI: 10.1021/nl504399d
Nano Lett. 2015, 15, 1722−1729